

Local order variations in confined hard-sphere fluids

Kim Nygård,^{1, a)} Sten Sarman,^{2, b)} and Roland Kjellander^{1, c)}¹⁾ *Department of Chemistry and Molecular Biology, University of Gothenburg, SE-412 96 Gothenburg, Sweden*²⁾ *Department of Materials and Environmental Chemistry, Stockholm University, SE-106 91 Stockholm, Sweden*

(Dated: 5 May 2021)

Pair distributions of fluids confined between two surfaces at close distance are of fundamental importance for a variety of physical, chemical, and biological phenomena, such as interactions between macromolecules in solution, surface forces, and diffusion in narrow pores. However, in contrast to bulk fluids, properties of inhomogeneous fluids are seldom studied at the pair-distribution level. Motivated by recent experimental advances in determining anisotropic structure factors of confined fluids, we analyze theoretically the underlying anisotropic pair distributions of the archetypical hard-sphere fluid confined between two parallel hard surfaces using first-principles statistical mechanics of inhomogeneous fluids. For this purpose, we introduce an experimentally accessible ensemble-averaged local density correlation function and study its behavior as a function of confining slit width. Upon increasing the distance between the confining surfaces, we observe an alternating sequence of strongly anisotropic versus more isotropic local order. The latter is due to packing frustration of the spherical particles. This observation highlights the importance of studying inhomogeneous fluids at the pair-distribution level.

I. INTRODUCTION

Fluids confined between two surfaces at close distance are abundant in physical, chemical, and biological systems. The spatial confinement induces a complex microscopic ordering of the fluid, which depends on both the interactions between the fluid particles and the confining walls as well as the mutual interactions between the fluid particles. The microscopic structure of the fluid is of fundamental importance for a wide range of phenomena, such as the interactions between macromolecules or colloidal particles in solution,¹ apparent charge reversal of suspended particles due to many-body ion correlations,²⁻⁵ and like-charge attraction due to ion-ion correlations.⁶⁻⁸ Moreover, an accurate description of the dynamical properties of confined fluids, such as the diffusivity in narrow pores^{9,10} and the friction between surfaces suspended in fluids,¹¹ necessitates a good description of static structure of the fluid. The relevance of the topic is further highlighted by the development of novel technological applications based on confinement of fluids, such as ionogels.¹²

Fluids are disordered systems, which are characterized by short-range density variations known as the local structure of the fluid. In the case of bulk fluids of spherical particles, the isotropic density around a fluid particle is given by $n_0 g(r)$, with n_0 denoting the bulk number density, $g(r)$ the pair-distribution function (also called the radial distribution function), and r the dis-

tance from the particle center. The pair distributions are also directly related to thermodynamic quantities, thereby providing a formal connection between microscopic and macroscopic properties of the fluid.¹³ Moreover, pair distributions can be routinely determined experimentally by means of x-ray or neutron scattering, making them the single most important quantity for characterization of fluid properties.

For confined fluids, in turn, the local density is governed by a complex interplay between particle-wall and particle-particle interactions. Hence, the local density at position \mathbf{r}_1 around a particle with its center at position \mathbf{r}_2 is given by $n(\mathbf{r}_1)g(\mathbf{r}_1, \mathbf{r}_2)$, with $n(\mathbf{r}_1)$ denoting the number density profile and $g(\mathbf{r}_1, \mathbf{r}_2)$ the pair-distribution function. In comparison with bulk fluids, there are two notable differences due to the presence of the confining surfaces: (i) $n(\mathbf{r}_1)$ exhibits spatial variation and (ii) $g(\mathbf{r}_1, \mathbf{r}_2)$ is anisotropic, depending on the individual values of \mathbf{r}_1 and \mathbf{r}_2 rather than on the magnitude of their difference, $r_{12} = |\mathbf{r}_1 - \mathbf{r}_2|$. Moreover, while the properties of bulk fluids are routinely analyzed microscopically in terms of their pair distributions, studies on the pair distributions of confined fluids remain scarce.

Given their fundamental importance, one may question why the pair distributions of confined fluids have, to a large extent, been neglected so far? This neglect can primarily be attributed to two causes. First, although the theoretical framework was developed a long time ago,^{14,15} the determination of theoretical pair distributions in confined fluids has so far been considered a computationally demanding task. In fact, the vast majority of computational work has focused on the simpler and generally less accurate singlet distribution (i.e., the density profile), while explicit calculations of pair distributions in confined fluids have been reported only very

^{a)}kim.nygard@chem.gu.se^{b)}sarman@ownit.nu^{c)}rkj@chem.gu.se

seldom.^{16–22} Second, there has to date been a lack of experimental data for comparison at the pair-distribution level, and hence there has been no strong incentive to explicitly determine theoretical pair distributions of confined fluids. Experimental studies have instead focused on singlet distributions of confined fluids - either indirectly using surface-force experiments^{23–25} or directly using, e.g., x-ray scattering²⁶ or confocal microscopy.²⁷ However, recently we demonstrated an experimental approach based on x-ray scattering from colloid-filled nanofluidic channel arrays,²⁸ providing experimental access to confined fluids at the pair-distribution level in terms of anisotropic structure factors - in quantitative agreement with first-principles statistical mechanics of inhomogeneous fluids.²⁹

In this paper, we analyze theoretically the anisotropic structure factors of Ref. 29 in terms of the underlying pair distributions. As a model system we study the archetypical hard-sphere fluid confined between smooth and hard planar surfaces, which is a good approximation for entropy-dominated fluids. The first-principles theoretical calculations are carried out within integral-equation theory, by solving the inhomogeneous Ornstein-Zernike and Lovett-Mou-Buff-Wertheim equations using the anisotropic Percus-Yevick closure.^{17,30} The main results of the paper are two-fold: First, we show that the experimentally accessible anisotropic structure factor can be interpreted in terms of an ensemble-averaged local density correlation function of the confined fluid. Next, we use this result to interpret the experimental findings of Ref. 29 as evidence for an alternating sequence of highly anisotropic, periodically modulated versus a more isotropic local order upon increasing the separation between the confining surfaces. In essence, this effect is driven by packing frustration, i.e., an incompatibility between the preferred local order of the fluid and the layering induced by the confining surfaces. The direct observation of a hitherto unknown sequence of local ordering-disordering phenomena on the pair-distribution level in the extensively studied system of a hard-sphere fluid between hard planar surfaces emphasizes the importance of explicitly studying inhomogeneous fluids at this level.

II. METHODS

A. Inhomogeneous integral-equation theory

The interaction potentials for the system with hard spheres between two hard surfaces are given by the particle-particle interaction potential,

$$\beta u(\mathbf{r}_1, \mathbf{r}_2) = \begin{cases} 0 & \text{if } |\mathbf{r}_1 - \mathbf{r}_2| \geq \sigma \\ \infty & \text{if } |\mathbf{r}_1 - \mathbf{r}_2| < \sigma \end{cases} \quad (1)$$

and the particle-wall potential,

$$\beta v(z) = \begin{cases} 0 & \text{if } |z| \leq L/2, \\ \infty & \text{if } |z| > L/2, \end{cases} \quad (2)$$

with $\beta = (k_B T)^{-1}$, k_B Boltzmann's constant, and T the absolute temperature. Here, the z -axis is placed perpendicular to the confining surfaces with its origin midway in between, while the particle centers are confined to a reduced slit width of $L = H - \sigma$, with H denoting the surface separation and σ the particle diameter.

In the calculations the planar symmetry of the system has been utilized. This reduces the spatial dimension of the density distribution $n(\mathbf{r})$ from three to one and the pair-distribution functions from six to three, for example $g(\mathbf{r}_1, \mathbf{r}_2) = g(z_1, z_2, R_{12})$, where $R_{12} = |\mathbf{R}_{12}|$ and $\mathbf{R}_{12} = (x_2 - x_1, y_2 - y_1)$. The density profile, the total correlation function $h(\mathbf{r}_1, \mathbf{r}_2) = h(z_1, z_2, R_{12}) = g(z_1, z_2, R_{12}) - 1$, and the direct correlation function $c(\mathbf{r}_1, \mathbf{r}_2) = c(z_1, z_2, R_{12})$ are obtained by solving the following set of equations: the Lovett-Mou-Buff-Wertheim equation,

$$\frac{d[\log n(z_1) + \beta v(z_1)]}{dz_1} = \int c(z_1, z_2, R_{12}) \frac{dn(z_2)}{dz_2} dz_2 d\mathbf{R}_{12}, \quad (3)$$

and the inhomogeneous Ornstein-Zernike equation,

$$h(\mathbf{r}_1, \mathbf{r}_2) = c(\mathbf{r}_1, \mathbf{r}_2) + \int h(\mathbf{r}_1, \mathbf{r}_3) n(z_3) c(\mathbf{r}_3, \mathbf{r}_2) d\mathbf{r}_3, \quad (4)$$

subject to the anisotropic Percus-Yevick (PY) closure

$$c(\mathbf{r}_1, \mathbf{r}_2) = g(\mathbf{r}_1, \mathbf{r}_2) - y(\mathbf{r}_1, \mathbf{r}_2), \quad (5)$$

where $y(\mathbf{r}_1, \mathbf{r}_2)$ is the cavity function that satisfies

$$g(\mathbf{r}_1, \mathbf{r}_2) = y(\mathbf{r}_1, \mathbf{r}_2) \exp[-\beta u(\mathbf{r}_1, \mathbf{r}_2)]. \quad (6)$$

The PY closure is the only approximation made. The set of Eqs. (3) - (6) is solved fully self-consistently in an iterative manner.

In the calculations the cavity function y is determined numerically on a grid. The number of grid points can thereby be kept to a minimum, since this function is continuous at the hard core periphery of the spheres. The pair-distribution function is then obtained from Eq. (6).

B. Boundary conditions

To solve Eq. (3), one needs a boundary condition for the density profile or some other suitable information. There are two particularly convenient choices: the number of particles per unit area in the slit, $N = \int_{-L/2}^{L/2} n(z) dz$, or the value of the density at some point, for instance the contact density at a wall surface $n(\pm L/2)$ or the value at the midpoint between the surfaces $n(0)$. One must, however, know what value to use when the fluid in the slit is in equilibrium with a bulk fluid of given density, which is a nontrivial problem within most integral equation theories at the anisotropic pair distribution level.³¹ We used the following method to determine this value for various surface separations.

The rate of change of the profile when the surface separation is changed under the condition of constant chemical potential is given by the exact equation^{17,30}

$$\frac{\partial n(z_1; L)}{\partial L} = -\beta n(z_1; L) \left[\frac{\partial v(z_1; L)}{\partial L} + \int n(z_2; L) \times h(z_1, z_2, R_{12}; L) \frac{\partial v(z_2; L)}{\partial L} dz_2 d\mathbf{R}_{12} \right], \quad (7)$$

where we have indicated explicitly that all functions depend on L [this notation is suppressed in Eqs. (3) - (6)]. By inserting v from Eq. (2) into Eq. (7) and integrating over z_1 , we obtain after simplification

$$\frac{dN(L)}{dL} = n(L/2; L) \left[1 + \int n(z_1; L) \times h(z_1, L/2, R_{12}; L) dz_1 d\mathbf{R}_{12} \right], \quad (8)$$

where we have used the symmetry with respect to the midplane between the surfaces. This is formally a first order differential equation for N as a function of L at constant chemical potential, i.e., $dN/dL = f(N, L)$, where f is the right-hand side of Eq. (8) that implicitly depends on N . In order to solve it we must have a boundary value $N_0 = N(L_0)$ for N , where L_0 is some suitable slit width. This value can be obtained by selecting a large L_0 so the density oscillations in the middle of the slit have decayed to a large extent and the density there virtually coincides with the bulk density, i.e., $n(0) = n_0$. Thereby, one solves Eqs. (3) - (6) for $L = L_0$ by using a value $N = N_0$ such that $n(0) = n_0$ is fulfilled. The value N_0 thus obtained can be used as boundary value for the integration of Eq. (8) to smaller slit widths where the fluid consequently will be in equilibrium with a bulk fluid of density n_0 . To evaluate $f(N, L)$ one must solve Eqs. (3) - (6) self-consistently at every step in L during the numerical integration of Eq. (8) with $N = N(L)$ as boundary condition for Eq. (3). In this manner we obtain the density profiles and pair-distribution functions for all wall separations $L \leq L_0$.

C. Computational details

In practice, the numerical solution procedure for Eqs. (3) - (6) and (8) starts by calculating the density profile and the pair-correlation functions for a wide slit of width L_0 , in our case $L_0 = 15\sigma$. For this surface separation, $N = N_0 = 11.8\sigma^{-2}$ gives the desired value of $n(0)$, i.e., $n_0 = 0.75\sigma^{-3}$. The iterational procedure for this initial solution of Eqs. (3) - (6) is started with a constant density profile and pair-correlation functions that are set equal to zero. About five CPU-hours are needed for convergence using eight nodes with a clock frequency of 2.6 GHz on a parallel machine. The cut-off radius is 6.4σ in r -space and $98\sigma^{-1}$ in k -space; 200 grid point are applied which give a step Δr and Δk of about 0.032σ and

$0.49\sigma^{-1}$, respectively. In the z -direction the step length Δz of the grid is equal to 0.025σ .

Once the density profile and the pair-correlation functions have been obtained, Eq. (8) is used to obtain a new value of N for $L = L_0 - \Delta L$, where $\Delta L = 2\Delta z = 0.05\sigma$. Thereby, one can utilize a numerical method such as, for example, the Runge-Kutta method, which we have chosen here. Equations (3) - (6) are solved again for this slit width and the new value of N . Then the whole procedure is repeated for $L - \Delta L$ etc. The start values for the density profile at each new slit width are obtained from Eq. (7), which gives a rather accurate new profile, and the old pair-correlation functions are used as start values for the new ones. Thanks to these good start values in the iterations the convergence becomes very fast, so only another five CPU-hours are needed to obtain self-consistent pair-correlation functions and density profiles for all the slit widths at interval ΔL down to one hard sphere diameter. Note that the algorithm parallelizes very well so it can be even faster if more cores are used in the computer.

III. RESULTS AND DISCUSSION

A. Anisotropic structure factor

In a physically appealing picture, the experimentally accessible anisotropic structure factor $S(\mathbf{q})$ of Refs. 28 and 29 is given by [see the Appendix for details, Eqs. (A.1) and (A.2)]

$$S(\mathbf{q}) = 1 + \int \langle n(\mathbf{r})h(\mathbf{r}, \mathbf{0}) \rangle e^{i\mathbf{q}\cdot\mathbf{r}} d\mathbf{r}, \quad (9)$$

with \mathbf{q} denoting the scattering vector. The coordinate system is here placed with the origin at the center of a particle, coordinate $\mathbf{0}$, and follows the particle during its motion. The vector \mathbf{r} is a position vector that starts from the particle center. The brackets depict an average over all particles in the slit, i.e., $\langle n(\mathbf{r})h(\mathbf{r}, \mathbf{0}) \rangle$ denotes the correlation function for the density distribution around a particle, averaged over all particle positions and weighted with the probability of finding each particle there [cf. Eq. (A.3)]. In other words, the anisotropic $S(\mathbf{q})$ probes in a direct manner the ensemble-averaged local density correlations in the confined fluid. In the rest of the paper we will denote $\langle n(\mathbf{r})h(\mathbf{r}, \mathbf{0}) \rangle$ as the averaged local density correlation function.

The visualization of $S(\mathbf{q})$ warrants a brief comment. Since the system has planar symmetry, we can without loss of generality write the density profile as $n(\mathbf{r}) = n(z)$ and the total pair-correlation function as $h(\mathbf{r}, \mathbf{0}) = h(z, R, \mathbf{0})$. Here, the z axis is perpendicular to the surfaces, $R = |\mathbf{R}|$, and $\mathbf{R} = (x, y)$ is directed parallel to the surfaces, i.e., \mathbf{R} is the in-plane component of \mathbf{r} . Therefore, Eq. (9) simplifies to

$$S(q_{\perp}, q_{\parallel}) = 1 + \int \langle n(z)h(z, R, \mathbf{0}) \rangle e^{i(q_{\perp}z + \mathbf{q}_{\parallel}\cdot\mathbf{R})} dz d\mathbf{R}, \quad (10)$$

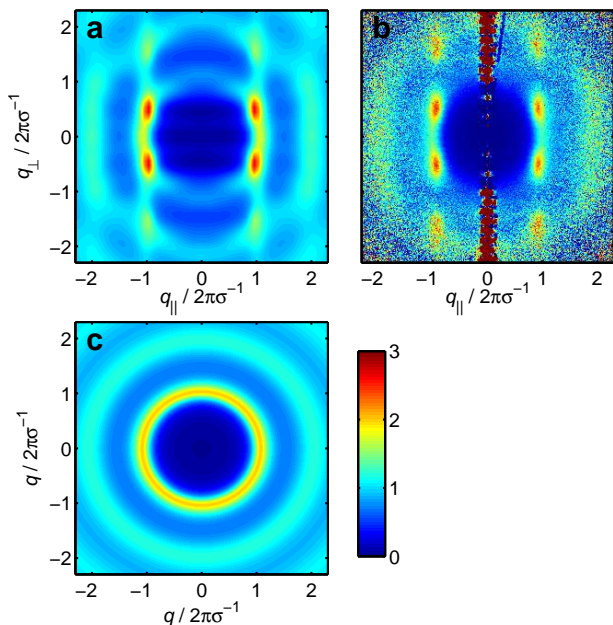


FIG. 1. Anisotropic structure factor for a hard-sphere fluid confined between hard planar surfaces. (a) Theoretical and (b) experimental $S(q_{\perp}, q_{\parallel})$ are shown for a reduced slit width of $L = 2.10\sigma$ and bulk number density $n_0 = 0.75\sigma^{-3}$. The dark red feature at $q_{\parallel} = 0$ in the experimental data is diffraction from the confining channel array, which should be neglected in the comparison. The experimental data are taken from Ref. 29. (c) The corresponding isotropic bulk $S(q)$ for $n_0 = 0.75\sigma^{-3}$.

where q_{\perp} and \mathbf{q}_{\parallel} denote the out-of-plane and in-plane components of the scattering vector, respectively, and $q_{\parallel} = |\mathbf{q}_{\parallel}|$. Throughout this paper, we plot for clarity also negative values of R . In these plots, R should be interpreted as a coordinate along a straight line in the xy plane through the origin.

Recently, we demonstrated a remarkable agreement between experimental and theoretical anisotropic structure factors $S(q_{\perp}, q_{\parallel})$ for a hard-sphere fluid confined between hard planar surfaces.²⁹ The quantitative agreement is for convenience exemplified in Fig. 1 for a reduced slit width of $L = 2.10\sigma$. Here, and throughout this study, the confined fluid is kept in equilibrium with a bulk fluid reservoir, with the bulk number density $n_0 = 0.75\sigma^{-3}$. For comparison, we also present the corresponding bulk structure factor $S(q)$, where $q = |\mathbf{q}|$. The latter is obtained by solving the isotropic Ornstein-Zernike equation within the PY approximation, i.e., the isotropic counterparts of Eqs. (4), (5), and (6), and using the hard particle-particle interaction potential in Eq. (1).¹³ In contrast to the bulk $S(q)$, both theoretical and experimental $S(q_{\perp}, q_{\parallel})$ exhibit anisotropy, most strongly manifested as distinct peaks around $(q_{\perp}, q_{\parallel}) \sim (\pm 1/2, \pm 1)$ (in units of $2\pi\sigma^{-1}$) and lobes at larger scattering vectors. The excellent agreement between theoretical and experimental $S(q_{\perp}, q_{\parallel})$ as shown here (and for several

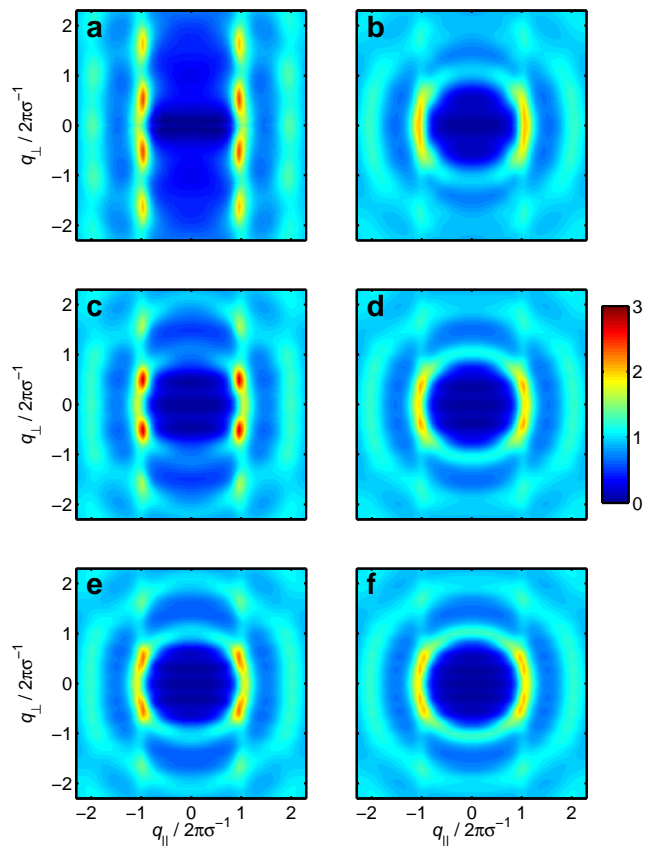


FIG. 2. Theoretical anisotropic structure factor as in Fig. 1, but for different slit widths. The reduced slit widths are (a) $L = 1.05\sigma$, (b) 1.60σ , (c) 2.05σ , (d) 2.55σ , (e) 3.00σ , and (f) 3.50σ .

slit widths in Ref. 29) evidence the accuracy, at the pair-distribution level, of the adopted theoretical scheme.

In order to gain further insight into the slit-width dependence of the ensemble-averaged local density correlation function in the confined fluid, we present in Fig. 2 the theoretical structure factor for a broad range of confining slit widths. Upon increasing the slit width, we observe an intriguing sequence of appearances and disappearances of distinct peaks in $S(q_{\perp}, q_{\parallel})$ [see Video 1 in the supplementary material for a larger set of $S(q_{\perp}, q_{\parallel})$ plots³²]. Since $S(q_{\perp}, q_{\parallel})$ is given by the Fourier transform of the ensemble-averaged local density correlation function $\langle n(z)h(z, R, \mathbf{0}) \rangle$ according to Eq. (10), this observation directly implies an alternating sequence of local structural ordering-disordering with increasing slit width.

We emphasize that the sequence of local ordering-disordering phenomena of Fig. 2 is not observable in the traditionally studied density profiles of confined fluids. This is exemplified in Fig. 3, which presents the number density profile $n(z)$ for various slit widths. The layered structure between the walls is developed maximally for surface separations that are close to an integer multiple of the sphere diameter, while for intermediate surface separations the layering is less well developed.

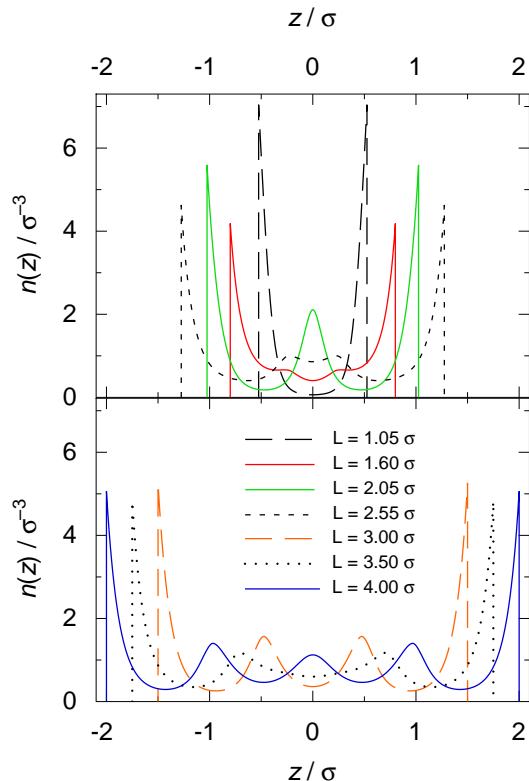


FIG. 3. Number density profiles $n(z)$ for the hard-sphere fluid confined between hard planar surfaces. The reduced slit widths range from $L = 1.05\sigma$ to 4.00σ .

We note that the two shoulders in the profile for $L = 1.60\sigma$ (red curve) have also been found in grand canonical simulations.³³ The adsorption excess of particles between the surfaces, defined as $\Gamma = \int_{-L/2}^{L/2} [n(z) - n_0] dz$ and displayed in Fig. 4, has peaks at the separations with maximal layering and troughs when the layering is weak. The average volume fraction of hard spheres in the slit, $\phi_{av} = (\pi\sigma^3/6H) \int_{-L/2}^{L/2} n(z) dz$, also presented in Fig. 4, shows a similar pattern. The chosen slit widths in Fig. 2 coincide approximately with subsequent maxima [Figs. 2(a), 2(c), and 2(e)] and minima [Figs. 2(b), 2(d), and 2(f)] in the adsorption excess Γ .

Importantly, while the peaks in $n(z)$ are more diffuse for slit widths close to minima compared to maxima in Γ , the density profiles of Fig. 3 do not exhibit any qualitative changes with increasing slit width which could be interpreted as signatures of local ordering-disordering phenomena at the pair-distribution level. Clearly, much can still be learned about confined fluids, even the extensively studied hard-sphere fluid between hard planar surfaces, by probing the system at the pair-distribution level.

It should be noted that $S(q_{\perp}, q_{\parallel})$ of the disordered fluid is qualitatively different during the transition from 2 \rightarrow 3 particle layers [Fig. 2(b)] compared to the subsequent

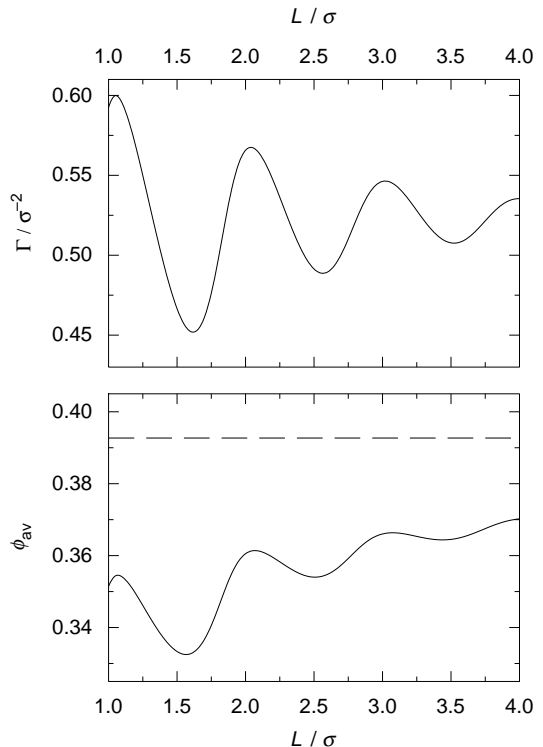


FIG. 4. Excess adsorption Γ and average volume fraction ϕ_{av} of hard spheres in the slit between two surfaces as functions of surface separation. The dashed curve shows the volume fraction in bulk.

transitions from 3 \rightarrow 4 [Fig. 2(d)] and 4 \rightarrow 5 particle layers [Fig. 2(f)]. In particular, the former $S(q_{\perp}, q_{\parallel})$ exhibits maxima at $(q_{\perp}, q_{\parallel}) \sim (0, \pm 2\pi\sigma^{-1})$, in contrast to the latter two cases, indicating a qualitative change in the packing frustration of particles for $L \approx 2\sigma$. Indeed, a careful inspection of the number density profiles of Fig. 3 (see Video 2 in the supplementary material for a larger set of slit widths³²) verifies this assertion. The transition from 2 \rightarrow 3 particle layers is found to proceed via buckling of the particle layers next to the solid surfaces, akin to so-called buckling transitions in thin crystalline films³⁴⁻³⁶ (for a review on buckling transitions, we refer the reader to Ref. 37). In contrast, the new particle layers are formed in the center of the slit during subsequent layering transitions. It should be noted, however, that the peaks at $(q_{\perp}, q_{\parallel}) \sim (0, \pm 2\pi\sigma^{-1})$ in $S(q_{\perp}, q_{\parallel})$ are observable only in a very narrow range of slit widths, $L \approx 1.60\sigma - 1.70\sigma$. Moreover, minor deviations from the ideal system studied here, such as size polydispersity of particles and not perfectly parallel planar walls in the experimental system, may preclude observation of this subtle packing effect. Consequently, the peaks at $(q_{\perp}, q_{\parallel}) \sim (0, \pm 2\pi\sigma^{-1})$ in $S(q_{\perp}, q_{\parallel})$ were not experimentally observed in Ref. 29.

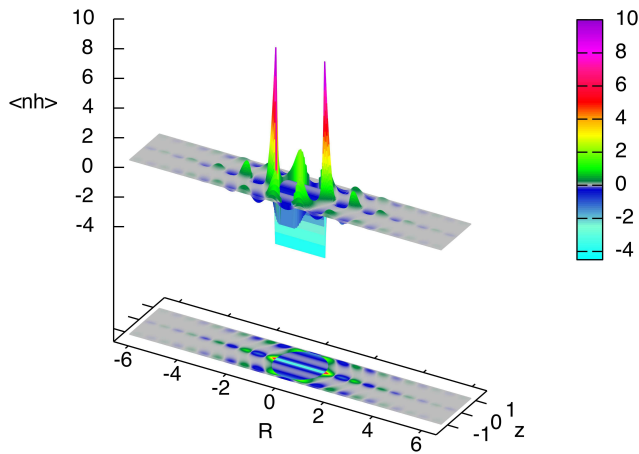


FIG. 5. Ensemble-averaged local density correlation function $\langle n(z)h(z, R, \mathbf{0}) \rangle$ for the reduced slit width $L = 1.05\sigma$. In the bottom part of the figure a contour plot of the function is shown and in the top part the same plot is illustrated in a 3D manner with peak heights proportional to the function value. The gray color denotes a narrow interval around the value zero.

B. Anisotropic local order

In order to obtain a real-space picture of the local structural order, we present in Fig. 5 the ensemble-averaged local density correlation function $\langle n(z)h(z, R, \mathbf{0}) \rangle$ for the reduced slit width of $L = 1.05\sigma$. The differences compared to the bulk counterpart $n_0h(r)$ are striking. First, the packing of particles leads to highly anisotropic, periodically modulated local density correlations, in stark contrast to the isotropic bulk counterpart. Second, the peaks in $\langle n(z)h(z, R, \mathbf{0}) \rangle$ are significantly more pronounced compared to the bulk $n_0h(r)$, indicative of the enhanced local order in the former case. Third, $\langle n(z)h(z, R, \mathbf{0}) \rangle$ exhibits structure inside the excluded volume around position $\mathbf{0}$, in contrast to bulk fluids. This latter phenomenon can be understood as follows. The pair-distribution function $g(z, R, \mathbf{0})$ vanishes within the excluded volume around $\mathbf{0}$. Consequently, the change in local order, relative to the average structure $n(z)$, becomes $\langle n(z)g(z, R, \mathbf{0}) - n(z) \rangle = \langle n(z)h(z, R, \mathbf{0}) \rangle$, which equals $-\langle n(z) \rangle$ for $z^2 + R^2 < \sigma^2$. For bulk fluids $\langle n(z) \rangle$ is simply a constant, whereas for confined fluids it is in essence an autocorrelation of $n(z)$, leading to the negative and R -independent periodic structure inside the excluded volume in the latter case. We emphasize that the complexity of $\langle n(z)h(z, R, \mathbf{0}) \rangle$, as presented here, hampers simple analysis of the ensuing $S(q_\perp, q_\parallel)$; a proper analysis of experimental structure factors from confined fluids, whether colloidal suspension in slits^{28,29} or molecular liquids confined in mesostructured porous matrices,^{38,39} necessitates the calculation of the underlying pair distributions theoretically.

Now we are in a position to analyze the slit-width dependence of the structure factor. In Fig. 6, we present

the ensemble-averaged local density correlation function $\langle n(z)h(z, R, \mathbf{0}) \rangle$ for the slit widths of Fig. 2 (see Videos 3 and 4 in the supplementary material for a larger set of $\langle n(z)h(z, R, \mathbf{0}) \rangle$ plots³²). The complex pattern around the central particle at the origin arises from a compromise between a planar layering of particles between the surfaces and a spherical layering induced by the particle. As anticipated based on $S(q_\perp, q_\parallel)$, we observe a sequence of local ordering in $\langle n(z)h(z, R, \mathbf{0}) \rangle$, with the fluid alternating between a periodic density pattern when the central particle penetrates layers that are in a quite ordered state and a more isotropic, bulk-like density pattern when the layers are in a more disordered (i.e., frustrated) state.

We note that the strong anisotropy observed for surface separations close to an integer multiple of the particle diameter [Figs. 6(a), 6(c), and 6(e)] is much less developed for $L > 3.0\sigma$. The plot for $L = 4.0\sigma$ (see Videos 3 and 4 in the supplementary material³²) shows only slightly more structure than that for $L = 3.5\sigma$, Fig. 6(f). Similarly, the corresponding $S(q_\perp, q_\parallel)$ plots in Fig. 2 (and in Video 1³² in the supplementary material) become more bulk-like for $L > 3.0\sigma$ [cf. Fig. 1(c)], with the distinct peaks around $(q_\perp, q_\parallel) \sim (\pm\pi\sigma^{-1}, \pm 2\pi\sigma^{-1})$ becoming strongly suppressed and the lobes at larger scattering vectors becoming nearly isotropic. Intriguingly, recent theoretical work on the diffusivity in confined hard-sphere fluids has revealed a similar slit-width dependence, with the oscillatory behavior of the diffusion coefficients as a function of slit width being strongly suppressed for $L > 3\sigma$.^{9,10} On a microscopic level, the diffusivity depends on the local density of the confined fluid; more ordered fluids have a larger free volume and hence a larger diffusivity.⁹ However, more theoretical work is needed in order to formally connect the $\langle n(z)h(z, R, \mathbf{0}) \rangle$'s of Fig. 6 to the findings of Refs. 9 and 10.

We also observe a subtle, yet important, difference in Fig. 6 between the local density correlation $\langle n(z)h(z, R, \mathbf{0}) \rangle$ of the disordered fluids, which leads to the qualitatively different behavior of the peaks in $S(q_\perp, q_\parallel)$ as discussed above, namely, the peaks located at $(q_\perp, q_\parallel) \sim (0, \pm 2\pi\sigma^{-1})$ for separations $L \approx 1.60\sigma - 1.70\sigma$, which are split into two peaks each with nonzero q_\perp for other surface separations. In Figs. 6(d) and 6(f), $L = 2.55\sigma$ and 3.50σ , we observe spatial correlations between particles in neighboring layers, similar to the sixfold correlations observed for $L = 1.05\sigma, 2.05\sigma$, and 3.00σ [Figs. 6(a), 6(c), and 6(d)], but less pronounced (keep in mind that the present system exhibits planar symmetry). For $L = 1.60\sigma$ [Fig. 6(b)], on the other hand, the peaks are smeared out in the z direction, which leads to the peaks in $S(q_\perp, q_\parallel)$ at zero q_\perp .

C. Anisotropic local density

The local correlation function $\langle n(z)h(z, R, \mathbf{0}) \rangle$, which is an ensemble average over all particles in the slit, can be decomposed into underlying local densities $n(\mathbf{r}_1)g(\mathbf{r}_1, \mathbf{r}_2)$

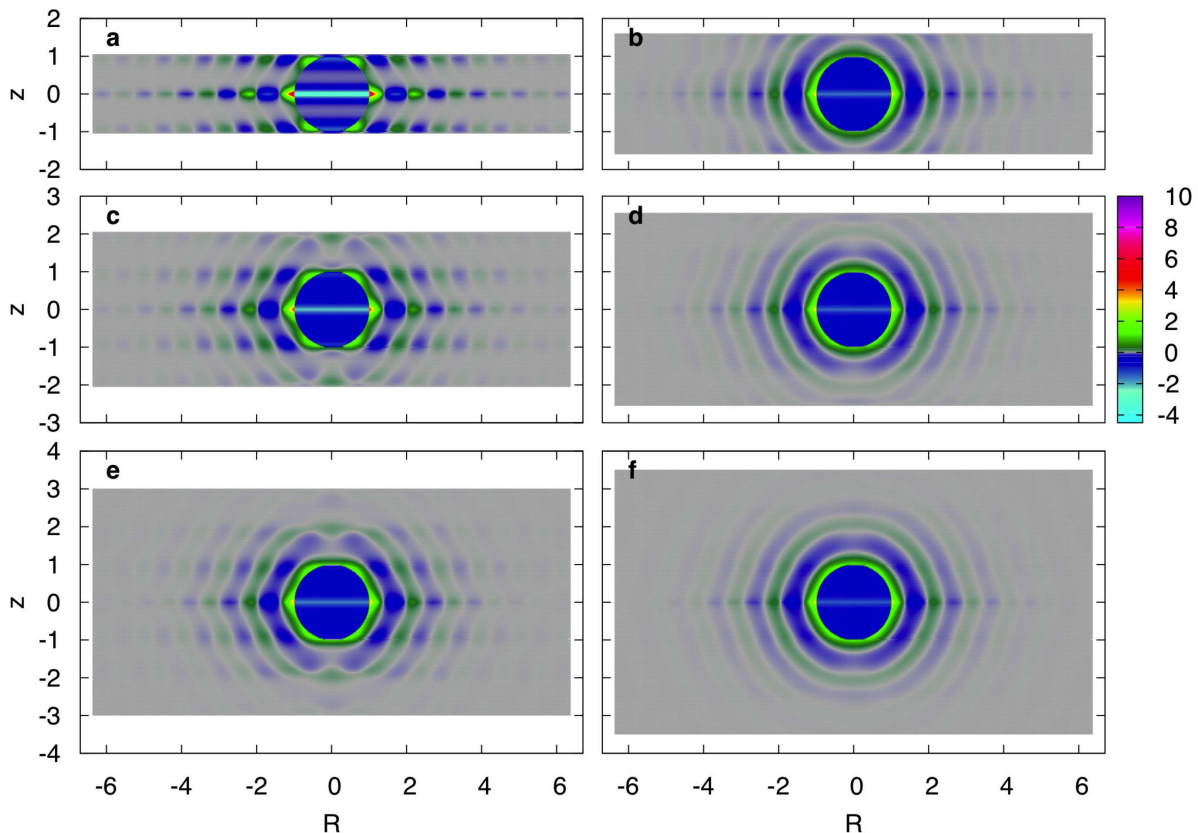


FIG. 6. Ensemble-averaged local density correlation function $\langle n(z)h(z, R, \mathbf{0}) \rangle$ corresponding to the anisotropic structure factors of Fig. 2. The reduced slit widths are (a) $L = 1.05\sigma$, (b) 1.60σ , (c) 2.05σ , (d) 2.55σ , (e) 3.00σ , and (f) 3.50σ .

for various particle positions \mathbf{r}_2 [see the Appendix and Eq. (A.3) below for the relationship between these kinds of entities]. To facilitate the understanding of the meaning of $\langle nh \rangle$ we here present the function ng for a few cases (in Ref. 17 some other plots of this function can be found for a somewhat lower bulk density). Due to planar symmetry, we have $n(\mathbf{r}_1)g(\mathbf{r}_1, \mathbf{r}_2) \equiv n(z_1)g(z_1, z_2, R_{12})$ where $R_{12} = |\mathbf{R}_{12}|$ and $\mathbf{R}_{12} = (x_1 - x_2, y_1 - y_2)$, so R_{12} denotes the in-plane projection of $|\mathbf{r}_1 - \mathbf{r}_2|$. In graphical representations of this function, it is convenient to let the z axis go through the particle center, i.e., we select $\mathbf{r}_2 = (0, 0, z_2)$. Then the function $n(z_1)g(z_1, z_2, R_{12})$ states the density at a point $\mathbf{r}_1 = (\mathbf{R}_{12}, z_1) = (x_1, y_1, z_1)$, when a particle is located at $(0, 0, z_2)$. Again, we plot for clarity also negative values of R_{12} , i.e., in the following plots R_{12} is to be interpreted as a coordinate along a straight line in the xy plane through the origin.

In Fig. 7, we show examples of the local density $n(z_1)g(z_1, z_2, R_{12})$ for the reduced slit width $L = 2.05\sigma$. In these plots, the particle is positioned (a) in contact with one surface at $z_2 = -1.025\sigma$, (b) at the density minimum at $z_2 = -0.475\sigma$, and (c) in the slit center at $z_2 = 0$ (a density maximum). For more particle positions z_2 , we refer to Video 5 in the supplementary material.³² The anisotropy in local density depends strongly on the particle position z_2 , or more specifically on the packing

conditions for other particles given a particle at z_2 . Most notably, in Figs. 7(a) and 7(b) the particle density in the wedge-like section formed between the particle and the nearby wall is strongly enhanced, resulting in a local number density of up to $18.0\sigma^{-3}$ and $22.9\sigma^{-3}$, respectively. The excluded volumes of the particle and the wall meet there and form a section where other particles can come in but not pass through. Particles will remain there for a relatively long time because when they try to escape they will usually be pushed in again by collisions with the surrounding particles. We note that similar local density enhancements have also been observed in binary hard-sphere mixtures and discussed in terms of depletion interactions.²¹ The enhancement in the local density $n(z_1)g(z_1, z_2, R_{12})$ relative to the singlet density $n(z_1)$ is given by the pair-distribution function $g(z_1, z_2, R_{12})$. In the inner part of the wedge-like section for these two cases g reaches 3.2 and 4.1, respectively. For comparison, the maximum value of the local density in Fig. 7(c), where no such wedge-like sections induced by overlapping excluded volumes exist, is a factor of ~ 3 smaller compared to those of Figs. 7(a) and 7(b).

The consequences of the penetration of the central particle into the particle layers between the walls as seen in Fig. 7 are also apparent in $\langle n(z)h(z, R, \mathbf{0}) \rangle$ of Fig. 6(c). In particular, the six-fold correlations mentioned above

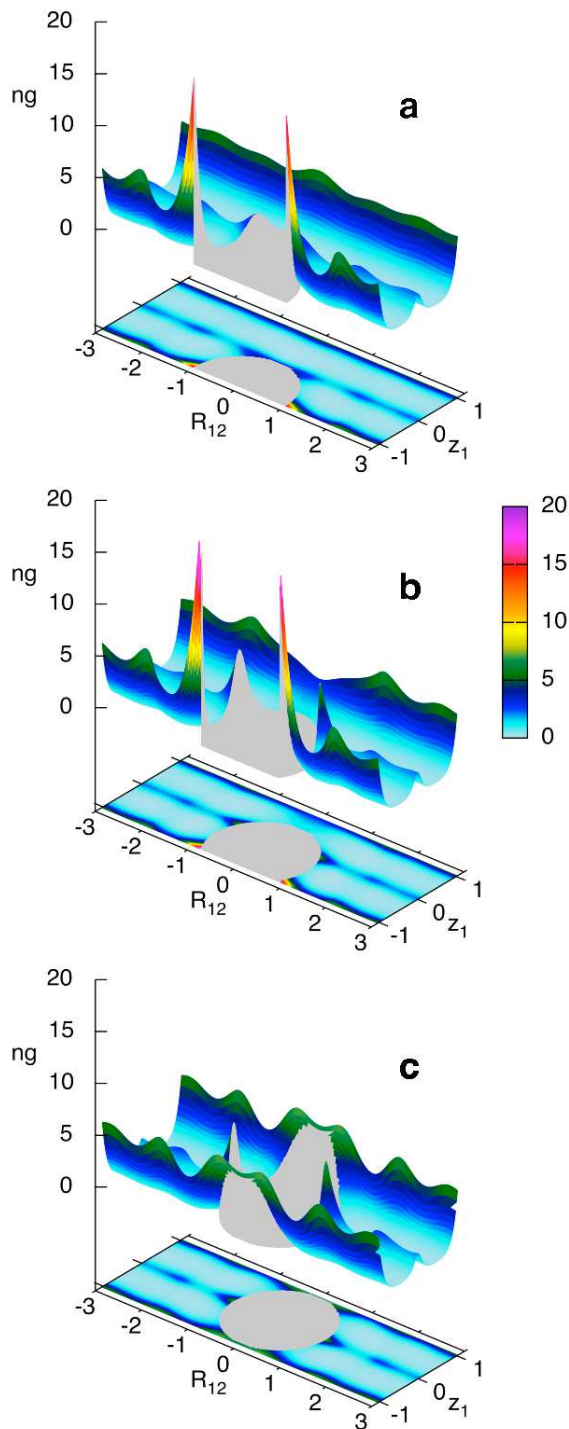


FIG. 7. Local density $n(z_1)g(z_1, z_2, R_{12})$ at coordinate (\mathbf{R}_{12}, z_1) around a particle in the slit between two hard surfaces, when the particle is located on the z axis at coordinate z_2 . Data are shown for the reduced slit width $L = 2.05\sigma$ and three different particle positions: (a) in contact with one surface, (b) at the density minimum, and (c) in the slit center. The gray region depicts the excluded volume around the particle.

are readily observed when the particle position z_2 is close to a density maximum like in Fig. 7(c). Note that the large peaks in $\langle n(z)h(z, R, \mathbf{0}) \rangle$ for $z = 0$ originate from $n(z_1)g(z_1, z_2, R_{12})$ with $z_1 = z_2$ for various particle positions z_2 . A major contribution to these peaks comes from the case with the particle in contact with a wall, Fig. 7(a), i.e., from the main density peaks at the wall which we discussed above. A substantial contribution also comes from cases like $z_2 = 0$, Fig. 7(c); in this case from the density peaks at $z_1 = 0$.

In the general case, a detailed quantitative analysis of local order in confined fluids based on $n(\mathbf{r}_1)g(\mathbf{r}_1, \mathbf{r}_2)$ may be a huge task, simply because of the large number of independent variables, \mathbf{r}_1 and \mathbf{r}_2 . As we have seen, there is a strong variation in both (i) $n(\mathbf{r}_1)g(\mathbf{r}_1, \mathbf{r}_2)$ with \mathbf{r}_1 and \mathbf{r}_2 and (ii) the probability of finding a particle at \mathbf{r}_2 [which is proportional to $n(\mathbf{r}_2)$]. This applies even when these functions can be calculated without undue effort. Analysis of $\langle n(\mathbf{r})h(\mathbf{r}, \mathbf{0}) \rangle$ is in this respect more convenient. Nevertheless, the explicit analysis of pair distributions is important for determining other properties of the system, such as the net force acting on a particle at various positions in the confined space.¹⁷

IV. CONCLUSION

The ensemble-averaged local density correlation function $\langle n(z)h(z, R, \mathbf{0}) \rangle$, as introduced and studied in this paper, exhibits two notable advantages. First, the local density $n(z_1)g(z_1, z_2, R_{12})$ is a multidimensional quantity, which depends on two positions relative to the confining surfaces; one of the positions is occupied by a particle and the other gives the position where the particle density is measured. In contrast, $\langle n(z)h(z, R, \mathbf{0}) \rangle$ is an ensemble average over all particles in the slit, which means that unlikely particle configurations are effectively filtered out. In essence, we have coarse-grained out one spatial dimension in $\langle n(z)h(z, R, \mathbf{0}) \rangle$ compared to $n(z_1)g(z_1, z_2, R_{12})$, which greatly facilitates the analysis of pair distributions in confined fluids. Second, $\langle n(z)h(z, R, \mathbf{0}) \rangle$ is directly accessible in x-ray scattering experiments, thereby allowing a quantitative comparison between experiment and theory in terms of the microscopic structure at the pair-distribution level. We foresee extensive studies of $\langle n(z)h(z, R, \mathbf{0}) \rangle$ for different particle-wall and particle-particle interaction potentials.

This study focuses on a simple model system – the extensively studied hard-sphere fluid confined between smooth and hard planar surfaces. However, the main finding reported here, a packing-frustration-induced alternating sequence of a strongly anisotropic, periodically modulated versus a more isotropic local order, is expected to be a general phenomenon. As mentioned in the Introduction, the hard-sphere fluid confined between hard surfaces can be regarded as a good approximation for entropy-dominated fluids: First, the pair distributions of simple dense fluids exhibiting short-ranged

particle-particle interactions are dominated by the excluded volume of the core region, which is contained in the present model. Second, short-ranged particle-wall interactions are dominated by the excluded volume at the interface, which is again included in the model. Further support for the generality of the observed ordering phenomenon is given by the following two examples: (i) anisotropic local densities $n(z_1)g(z_1, z_2, R_{12})$ resembling those presented in Fig. 7 have previously been reported for confined Lennard-Jones fluids¹⁸ and (ii) signatures in $S(q_\perp, q_\parallel)$ of local ordering, similar to those presented in Fig. 2, have been experimentally observed in a system of charged colloidal particles confined between charged surfaces.²⁸ We therefore expect the local ordering-disordering phenomenon as observed here to be an intrinsic property of a large class of dense simple fluids under spatial confinement.

Finally, we return to the computational effort alluded to in the Introduction. In this work, we have determined the anisotropic pair-distribution functions and the structure factor by application of integral-equation theory. In principle, these functions could also be evaluated directly from particle configurations obtained by grand-canonical Monte Carlo³³ or molecular dynamics⁴⁰ simulations. However, even with the computing power presently available, one would need impractically long simulations in order to obtain a reasonable statistical accuracy for the entire $n(\mathbf{r}_1)g(\mathbf{r}_1, \mathbf{r}_2)$. Alternatively, one can determine the pair distributions point-wise in simulations using the Widom insertion method, provided the fluid is not so dense that this method becomes too inefficient. Such a Monte Carlo approach has previously been compared with an integral-equation theory, similar to the one used here, in the case of inhomogeneous electrolytes;⁴¹ for the corresponding amount of pair-distribution data of essentially equal accuracy, the integral-equation approach was found to be many thousands times more efficient in CPU time than the simulations.

For the present work, the computations of all results presented were carried out in less than 10 hours of CPU time (see Sec. II for details). This included calculations of pair correlations and density profiles for all surface separations from $L = 15.00\sigma$ to 1.00σ with a resolution $\Delta L = 0.05\sigma$. Only a small fraction of these results is presented here. Hence, we see no genuine computational barriers precluding studies of confined fluids, or more generally inhomogeneous fluids, at the pair-distribution level. Similar conclusions were drawn in a recent computational study of electrolytes confined between two dielectric planar surfaces.²²

ACKNOWLEDGMENTS

R.K. and K.N. acknowledge support from the Swedish Research Council (Grant Nos. 621-2009-2908 and 621-2012-3897, respectively). The computations were sup-

ported by the Swedish National Infrastructure for Computing (SNIC 001-09-152) via PDC.

Appendix: Anisotropic structure factor

The experimentally accessible anisotropic structure factor of Refs. 28 and 29 is given by

$$S(\mathbf{q}) = 1 + \frac{1}{M} \int \int n(\mathbf{r}_1)n(\mathbf{r}_2)h(\mathbf{r}_1, \mathbf{r}_2)e^{i\mathbf{q}\cdot(\mathbf{r}_1-\mathbf{r}_2)} d\mathbf{r}_1 d\mathbf{r}_2, \quad (\text{A.1})$$

where M denotes the total number of particles in the confining slit ($M = NA$, where A is the area of the wall surface). In a more intuitive picture, $S(\mathbf{q})$ probes the local density correlation around a particle, averaged over all particles in the slit. Formally, this is obtained by averaging over all possible positions \mathbf{r}_2 across the confining channel, weighted with the probability density $p(\mathbf{r}_2) = n(\mathbf{r}_2)/M$ of finding the particle at position \mathbf{r}_2 . In practice, this is readily achieved by fixing the coordinate system $\mathbf{0}$ in Eq. (A.1) on the particle at position \mathbf{r}_2 , leading to

$$S(\mathbf{q}) = 1 + \int \langle n(\mathbf{r})h(\mathbf{r}, \mathbf{0}) \rangle e^{i\mathbf{q}\cdot\mathbf{r}} d\mathbf{r}, \quad (\text{A.2})$$

where $\langle \cdot \rangle$ is the average with respect to the probability density p and $\mathbf{r} = \mathbf{r}_{12} = \mathbf{r}_1 - \mathbf{r}_2$ is the position vector that starts from the particle center. The functions n and h have here been redefined and written with respect to the particle-centered coordinate system, i.e., $n(\mathbf{r}+\mathbf{r}_2) \Rightarrow n(\mathbf{r})$ and $h(\mathbf{r}+\mathbf{r}_2, \mathbf{r}_2) \Rightarrow h(\mathbf{r}, \mathbf{0})$. The ensemble-averaged local density correlation function can alternatively be written as

$$\langle n(\mathbf{r})h(\mathbf{r}, \mathbf{0}) \rangle = \int_{-(L+z-|z|)/2}^{(L-z-|z|)/2} w(z_2)n(z+z_2)h(z+z_2, z_2, R) dz_2, \quad (\text{A.3})$$

where the functions in the integrand are written with respect to the coordinate system with origin at the mid-plane of the slit, $w(z_2) = n(z_2)/N$ is the appropriate weight function, $\mathbf{r} = (\mathbf{R}, z)$, and $R = |\mathbf{R}|$. We note that the available space perpendicular to the confining surfaces equals $2L$ rather than L , since the largest possible out-of-plane distance between two particles is L in both positive and negative directions.

- ¹J. Israelachvili and H. Wennerström, *Nature* **379**, 219 (1996).
- ²G. M. Torrie and J. P. Valleau, *J. Phys. Chem.* **86** 3251 (1982).
- ³P. Kélicheff, S. Marčelja, T. J. Senden, and V. E. Shubin, *J. Chem. Phys.* **99**, 6098 (1993).
- ⁴R. Kjellander, *J. Phys.: Condens. Matter* **21**, 424101 (2009).
- ⁵A. Kubičková, T. Krížek, P. Coufal, M. Vazdar, E. Wernersson, J. Heyda, and P. Jungwirth, *Phys. Rev. Lett.* **108**, 186101 (2012).
- ⁶L. Guldbrand, B. Jönsson, H. Wennerström, and P. Linse, *J. Chem. Phys.* **80**, 2221 (1984).
- ⁷R. Kjellander and S. Marčelja, *Chem. Phys. Lett.* **112**, 49 (1984).
- ⁸R. Kjellander, S. Marčelja, R. M. Pashley, and J. P. Quirk, *J. Phys. Chem.* **92**, 6489 (1988).
- ⁹J. Mittal, T. M. Truskett, J. R. Errington, and G. Hummer, *Phys. Rev. Lett.* **100**, 145901 (2008).

- ¹⁰S. Lang, V. Bořan, M. Oettel, D. Hajnal, T. Franosch, and R. Schilling, *Phys. Rev. Lett.* **105**, 125701 (2010).
- ¹¹B. Bhushan, J. N. Israelachvili, and U. Landman, *Nature* **374**, 607 (1995).
- ¹²M.-A. Néouze, J. Le Bideau, P. Gaveau, S. Bellayer, and A. Vieux, *Chem. Mater.* **18**, 3931 (2006).
- ¹³J.-P. Hansen and I. R. McDonald, *Theory of Simple Liquids* (Academic Press, Amsterdam, 2006, 3rd ed).
- ¹⁴J. K. Percus in *The Equilibrium Theory of Classical Fluids* edited by H. L. Frisch and J. L. Lebowitz, II.33–II.170 (Benjamin, New York, 1964).
- ¹⁵S. Sokolowski, *J. Chem. Phys.* **73**, 3507 (1980).
- ¹⁶R. Kjellander and S. Marčelja, *J. Chem. Phys.* **88**, 7138 (1988).
- ¹⁷R. Kjellander and S. Sarman, *J. Chem. Soc. Faraday Trans.* **87**, 1869 (1991).
- ¹⁸R. Kjellander and S. Sarman, *Molec. Phys.* **74**, 665 (1991).
- ¹⁹B. Götzelmann and S. Dietrich, *Phys. Rev. E* **55**, 2993 (1997).
- ²⁰D. Henderson, S. Sokolowski, and D. Wasan, *J. Stat. Phys.* **89**, 233 (1997).
- ²¹V. Bořan, F. Pesth, T. Schilling, and M. Oettel, *Phys. Rev. E* **79**, 061402 (2009).
- ²²J. W. Zwanikken and M. Olvera de la Cruz, *Proc. Natl. Acad. Sci. USA* **110**, 5301 (2013).
- ²³R. G. Horn and J. N. Israelachvili, *J. Chem. Phys.* **75**, 1400 (1981).
- ²⁴J. N. Israelachvili, *Proc. Natl. Acad. Sci. USA* **84**, 4722 (1987).
- ²⁵S. H. L. Klapp, Y. Zeng, D. Qu, and R. von Klitzing, *Phys. Rev. Lett.* **100**, 118303 (2008).
- ²⁶M. J. Zwanenburg, J. H. H. Bongaerts, J. F. Peters, D. O. Riese, and J. F. van der Veen, *Phys. Rev. Lett.* **85**, 5154 (2000).
- ²⁷C. R. Nugent, K. V. Edmond, H. N. Patel, and E. R. Weeks, *Phys. Rev. Lett.* **99**, 025702 (2007).
- ²⁸K. Nygård, D. K. Satapathy, J. Buitenhuis, E. Perret, O. Bunk, C. David, and J. F. van der Veen, *EPL* **86**, 66001 (2009).
- ²⁹K. Nygård, R. Kjellander, S. Sarman, S. Chodankar, E. Perret, J. Buitenhuis, and J. F. van der Veen, *Phys. Rev. Lett.* **108**, 037802 (2012).
- ³⁰R. Kjellander and S. Sarman, *Chem. Phys. Lett.* **149**, 102 (1988).
- ³¹See R. Kjellander and S. Sarman, *J. Chem. Phys.* **90**, 2768 (1989), where it is shown that for most integral equation closures, including the PY closure, there exists no unique explicit expression for the chemical potential. The latter is, in fact, a path dependent quantity in these approximations. Therefore, it is not easy to obtain the density profile for a given chemical potential (same as in the bulk). In the anisotropic hypernetted chain (AHNC) approximation, on the other hand, a unique expression exists which can be utilized to calculate the density profile for a given chemical potential (see, e.g., Ref. 7). The AHNC approximation, which is suitable for systems with long-ranged interactions, is, however, not accurate for hard-sphere fluids.
- ³²See Supplemental Material at http://www2.chem.gu.se/~rkj/Suppl_mat_JCP_139/ for larger sets of slit widths.
- ³³J. Mittal, J. R. Errington, and T. M. Truskett, *J. Chem. Phys.* **126**, 244708 (2007).
- ³⁴S. Nesper, C. Bechinger, and P. Leiderer, *Phys. Rev. Lett.* **79**, 2348 (1997).
- ³⁵M. Schmidt and H. Löwen, *Phys. Rev. E* **55**, 7228 (1997).
- ³⁶A. Fortini and M. Dijkstra, *J. Phys.: Condens. Matter* **18**, L371 (2006).
- ³⁷H. Löwen, *Soft Matter* **6**, 3133 (2010).
- ³⁸F. Bruni, M. A. Ricci, and A. K. Soper, *J. Chem. Phys.* **109**, 1478 (1998).
- ³⁹D. Morineau and C. Alba-Simionesco, *J. Chem. Phys.* **118**, 9389 (2003).
- ⁴⁰J. Gao, W. D. Luedtke, and U. Landman, *Phys. Rev. Lett.* **79**, 705 (1997).
- ⁴¹H. Greberg, R. Kjellander, and T. Åkesson, *Molec. Phys.* **87**, 407 (1996).